

AD-A111 944

FOREIGN TECHNOLOGY DIV WRIGHT-PATTERSON AFB OH
LASER JOURNAL (SELECTED ARTICLES).(U)

F/G 20/5

UNCLASSIFIED

FEB 82
FTD-ID(RS)T-1390-81

NL

1 of 1
A-111 944



| | | | | | | | | | | | | |
|--|--|--|--|--|--|--|--|--|--|--|--|--|
| | | | | | | | | | | | | |
| | | | | | | | | | | | | |
| | | | | | | | | | | | | |

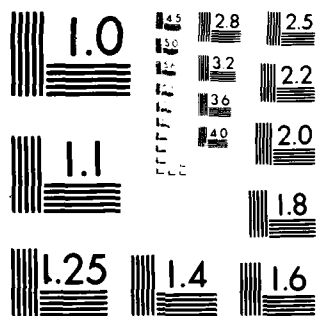
END

DATE

FILED

1-82

NTIC



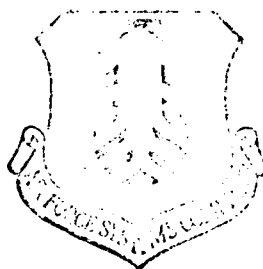
MICROCOPY RESOLUTION TEST CHART
NATIONAL BUREAU OF STANDARDS-1963-A

2

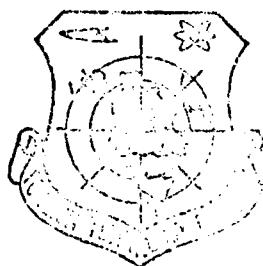
FD-10(AS) 1-79-91

ADA111944

FOREIGN TECHNOLOGY DIVISION



LASER JOURNAL
(Selected Articles)



DTIC
SELECTED
MAR 11 1982
S H

DTIC FILE COPY

Approved for public release;
distribution unlimited.

82 06 11 083

EDITED TRANSLATION

FTD-ID(RS)T-1390-81

12 February 1982

MICROFICHE NR: FTD-82-C-000181

LASER JOURNAL (Selected Articles)

English pages: 33

Source: Laser Journal, Vol. 8, Nr. 1, 1981, pp. 5-9; 10-13; 18-20;
47-48

Country of origin: China

Translated by: LEO KANNER ASSOCIATES
F33657-81-D-0264

Requester: FTD/TQTD

Approved for public release; distribution unlimited.

THIS TRANSLATION IS A RENDITION OF THE ORIGINAL FOREIGN TEXT WITHOUT ANY ANALYTICAL OR EDITORIAL COMMENT. STATEMENTS OR THEORIES ADVOCATED OR IMPLIED ARE THOSE OF THE SOURCE AND DO NOT NECESSARILY REFLECT THE POSITION OR OPINION OF THE FOREIGN TECHNOLOGY DIVISION.

PREPARED BY:

TRANSLATION DIVISION
FOREIGN TECHNOLOGY DIVISION
WP.AFB, OHIO.

FTD-ID(RS)T-1390-81

Date 12 Feb 19 82

Table of Contents

| | |
|---|----|
| Effect of Thermal Deformation in Mirrors on Resonator Parameters, by Zhang Xinchang, Sun Mengjia, and Guo Congjian | 1 |
| Folded Resonator for High Power Lasers, by Lei Shizhan, and Zhou Zhongyi | 12 |
| A Copper Vapor Laser, by Liang Baogen, Jing Chunyang, Zhang Guiyan, Yin Xanhua, Cang Yunching, and Han Shaochen | 21 |
| Experiments and Research of Electron Beam Control XeCl Quasi- Molecule Laser, by Hong Pu | 31 |



| | |
|--------------------|-------------------------------------|
| Accession For | |
| NTIS | <input checked="" type="checkbox"/> |
| DTIC | <input type="checkbox"/> |
| Unpublished | <input type="checkbox"/> |
| Justification | |
| By _____ | |
| Distribution/ | |
| Availability Codes | |
| Dist _____ | |
| A | |

EFFECT OF THERMAL DEFORMATION IN MIRRORS ON RESONATOR PARAMETERS

Zheng Xinchun, Sun Mengjie, and Guo Congjian

Shanxi University

Submitted 4 March 1980

Influence of thermal deformation in mirrors upon the resonator parameters is discussed. In designing a high-power laser and a folded-resonator CO_2 laser in particular, it must be considered in advance as much as possible.

When laser power is increased, thermal deformation in mirrors due to absorption wear-out is more apparent; this deformation becomes an important factor, affecting laser resonator parameters (in particular, more strongly folded CO_2 lasers). So this effect should be considered.

1. Experimental Details

We performed experiments with a 2-refer V-type folded CO_2 laser. Besides the output mirror, all reflection mirrors were made of ordinary optical glass on the base mirror. An infrared-focus-adjusting automatic collimator was used to measure (frontal, back of mirror) the variation in the radius of curvature. It was found that after laser operation, there was an apparent change in the curvature of these adjustment. When the back of the mirrors were coated with silver, and the difference between the focus adjustment radius of mirrors was measured, the degree of change in the (frontal, back adjustment) was

the distance. When the rotation is finished (point) the rotation plate in front of the camera is shifted to the position (with time) of the spot of the laser beam. The camera of the film is switched on, laser beam turned a circle back on the film and photo is taken in Figure 1. The width of spot around a mirror varied from 50 microns and 1 mm.

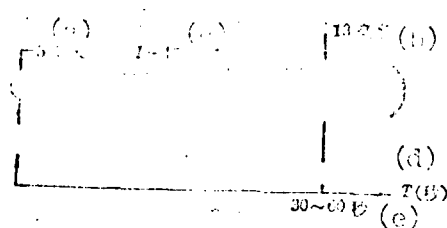


Fig. 1. Changes (with time) of laser output light-spot sizes.
Key: (a) 5 millimeters; (b) 13 millimeters; (c) 1.65 millimeters; (d) 1 (second); (e) 30-60 seconds.

We recognized that the difference in the light-spot sizes between the calculated value based on the cavity theory and the initial light spot at $t=0$ is caused by the lens-like effect of the working gas. The reason why the light spot slowly broadened with time is mainly caused by thermal deformation. Since the settling time of the lens-like effect of the gas can be estimated from the characteristic time during which the gas molecules diffuse from the center (of laser discharge tube) to the tube wall [1], and the estimated $\tau_{\text{diffusion}} \approx 0.1$ second applies to the working gas of CO_2 laser, it is apparent that the settling time of the lens-like effect (of gas) can be considered as instantaneous. The 30-second period in the experiments represents the settling time of the thermal deformation of the mirror.

Although the lens-like effect of the gas is apparent in a CO_2 laser tube longer than 2 meters, the focal distance required in experiments was more than 50 meters. In other, in the above experiments, there were considerable changes with time in the light-spot sizes. This explains why the effect of laser resonator caused by thermal deformation was more important than the thermal expansion of the gas. The thermal expansion of the gas was relatively small.

11. Thermal Deformation of Mirrors

The thermal conductivity of the end wall of a mirror (in a CO_2 laser) is also high, so that from another point of view it can be generally considered as an isothermal condition. In the case of film, the outer surface of the mirror also is kept at a certain constant temperature. Reflecting the small amount of heat carried away by the discharge tube walls, under the condition of thermodynamic equilibrium, the heat absorbed by the inner surface of the mirrors per unit time should be equal to the heat carried away by heat conduction through the mirror per unit of time.

$$P(1-\tau) = 4.18\beta \left(\frac{\partial T}{\partial x} \right) S \approx 4.18\beta \frac{\Delta T}{d} S$$

In the above one-dimensional thermal conduction equation, P represents power in the laser chamber; τ is the reflectivity of mirror; β is the coefficient of thermal conductivity of the mirror base plate, estimated at $\beta = 0.602$ calorie per centimeter-second-degree; $\partial T / \partial x$ represents the temperature gradient along the direction of tube axis, approximately considered as $(\partial T / \partial x)_0 (\Delta T / a)$; ΔT is the average temperature difference between the inner and outer surfaces of the mirror; d is the mirror thickness; and S is the mirror area (approximately equal to the cross-sectional area of the discharge tube). From the above equation, we derive

$$\Delta T \approx 120P(1-\tau) \frac{d}{S} = 120(1-\tau) \frac{Wd}{St} \quad (1)$$

In the equation, W is the laser output power and t is the transmissivity of the output window.

As shown in Fig. 2, R is the radius of curvature of the concave lens. At the axis, the radius vectors are drawn from O (the center of curvature) toward the mirror; the included angle between the two radius vectors is ϕ . The curve sector ($''$) at the outer surface of the mirror does not vary because of the constant cooling-water temperature. At the inner surface of mirror, an increase of ΔT in temperature is caused by the absorption of light energy. The curve sector was increased from $''$ to $'' + \Delta \phi$ ($'' = 174.4^\circ$). In the equation, α represents the thermal expansion coefficient of the mirror material; for V_2O_5 optical glass, $\alpha = 96 \times 10^{-7} \text{ } ^\circ\text{C}^{-1}$. After deformation, the radius of curvature (of mirror) was R' and the center of curvature shifted to O' . From geometrical relationship, we can derive the following:

$$R' = \frac{l}{\varphi} \frac{l_1(1 - \alpha \Delta T) - R(1 + \alpha \Delta T)}{R - d} \approx -\frac{Rd}{\alpha \Delta T l} \quad (2)$$

If the mirror is a plane lens, then

$$R' \approx -\frac{d}{\alpha \Delta T l} \quad (2)'$$

We can see that thermal deformation increases the radius of curvature of concave lens and changes a plane lens into a convex lens. So possible variation in the radius of curvature (of mirror) should be considered before designing a laser resonator. We call this a compensation design compensating for the thermally deformed resonator of the mirror.

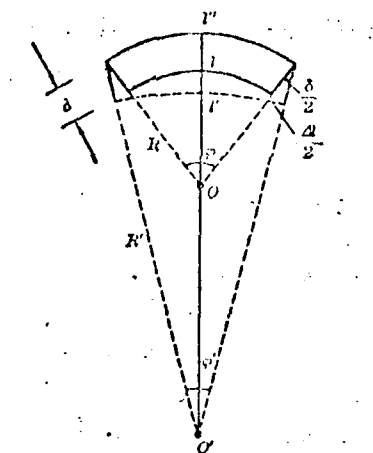


Fig. 2. Thermal deformation of mirror.

III. Effect on Resonator Parameters of Mirror Thermal Deformation

(A) Effect on straight channel

In a straight channel with length l and mirrors with radii of curvatures R_1 and R_2 , for the output mirror R_2 or its thermal conductivity is relatively high

INTRODUCTION. The effect of thermal deformation of mirrors on the parameters of a laser resonator is considered. After the deformation of the mirrors, the equivalent parameters of the resonator are determined.

$$g_1' = 1 - \frac{L}{R_1};$$

$$g_2' = \left(1 - \frac{L}{R_2}\right) + \frac{120\alpha L(1 - \tau)W}{St} = g_2 + MW_c;$$

$$M = \frac{120\alpha L(1 - \tau)Y}{St},$$

In the equation,

For a given mirror, L is a constant. We can see that the parameter g always linearly increases with M . Thus, the laser output light-spot becomes:

$$\omega' = \sqrt{\frac{L\lambda}{\pi}} \left[\frac{g_2'}{g_1(1 - g_1g_2')} \right]^{\frac{1}{4}};$$

$$= \sqrt{\frac{L\lambda}{\pi}} \left\{ \frac{g_2 + MW_c}{g_1[(1 - g_1g_2) - g_1MW_c]} \right\}^{\frac{1}{4}}.$$

(B) Effect on folded chamber

Since the number of lenses is increased, the effect of mirror thermal deformation on parameters is much more involved than for a straight chamber. By taking as an example a relatively simple V-type folded chamber as shown in Fig. 3, when $a_1 = a_2 = a$ and $R_1 = \infty$ (output of plane lens), the parameters of the equivalent chamber are derived as:

$$\begin{cases} N = \frac{a^2}{2\lambda L \left(1 - \frac{L}{R_3}\right)} \\ G_1 = 1 - \frac{2L}{R_3} \\ G_2 = 1 - \frac{2L}{R_3} - \frac{2L}{R_3} \left(1 - \frac{L}{R_3}\right) \end{cases}$$

When the chamber parameters become (after mirror thermal deformation) as follows:

$$\begin{cases} N = \frac{e^2}{2AL \left[\left(1 - \frac{L}{R_3}\right) + 2MW \right]} \\ G_1 = \left(1 - \frac{2L}{R_3}\right) + 4MW \\ G_2 = \left[\left(1 - \frac{2L}{R_3}\right) - \frac{2L}{R_2} \left(1 - \frac{L}{R_3}\right) \right] \\ \quad + 2M \left[\left(3 - \frac{2L}{R_2}\right) - \frac{L}{R_3} \right] W \\ \quad + 4M^2 W^2 \end{cases}$$

By using the correlation relationship [1] for the equivalent chamber G parameters and Fresnel number, we derived the following:

$$\begin{cases} g_1 = g_1 - 1 \\ g_2 = \left[\left(1 - \frac{2L}{R_3}\right) + 4MW \right] \left\{ \left[\left(1 - \frac{2L}{R_3}\right) - \frac{2L}{R_2} \left(1 - \frac{L}{R_3}\right) \right] \right. \\ \quad \left. + 2M \left[\left(3 - \frac{2L}{R_2}\right) - \frac{L}{R_3} \right] W \right. \\ \quad \left. + 4M^2 W^2 \right\} \end{cases} \quad (3)$$

From the above equations, the parameter G (or g) of the folded chamber also increases simply-linearly with the laser output power W ; however, the variation is much more apparent than for the straight chamber. The Fresnel number N decreases simply-hyperbolically with W ; i.e., the mirror thermal deformation always lowers the Fresnel number. Particularly noteworthy is the fact that there is a fairly close relationship between the Fresnel number for the straight chamber and the radius of curvature (R_3) of the folded mirror. The decrease in the Fresnel number is mainly caused by thermal deformation of the folded mirror. Therefore, when designing the folded chamber it is very important to properly select the radius of curvature of rotating mirrors. From the simple harmonic variation of chamber parameters with the laser output power W , thermal deformation of mirror can change a steady chamber into an unsteady chamber. Conversely, it is also possible to change an excessively concentrating unsteady chamber into a steady working chamber.

If the effect of the gas lens-like effect is neglected for the moment, the reflector of the cylindrical type of the FWHM radiating the same laser output is

$$\sigma = \sqrt{\frac{L}{\pi}} \left[1 + \frac{d^2}{q^2} \right]^{-1/2} \quad (4)$$

In this section, we will find the value of the equivalent diameter of V-type folded chamber. The expression

$$L = \frac{2L_1 \left[\left(1 - \frac{L_1}{R_1} \right) + 2MVF \right]}{\left[\left(1 - \frac{2L_1}{R_3} \right) + 4MVF \right]} \quad (5)$$

R_2^* is given in Equation (2).

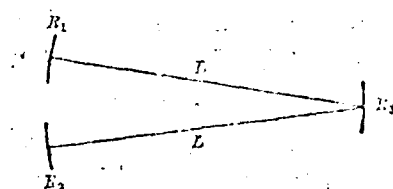


Fig. 3. V-type folded resonator

IV. Proof and Calculation

Then the folded chamber shown in Fig. 3, select different combinations of the mirrors; an experiment is conducted to prove the theoretical calculations above. Assume $L=2$ meters, $S=10$ centimeters², $d=0.5$ centimeter, and $t=45$ percent, and $(1-\tau)=1.4$ percent. From calculations, $R=6.72 \times 10^{-11}$. By applying plan number 1, $R_2=R_1=\infty$, $R_3=10$ meters, and $\sigma_1\sigma_2=0.36<1$; the cavity is a steady cavity. However, when $P=150$ watts, $\sigma_1\sigma_2=1.209>1$, the working chamber becomes an unsteady chamber because of thermal deformation. With this type of mirror combination (in a laser), the optimal laser power is less than 100 watts; moreover, when the discharge current is increased from 20 to 40 milliamperes, the laser output power has no apparent change. By slightly playing mirrors manually to change the cavity mode, the output power also has no apparent change. This phenomenon reveals that there is very considerable loss in the cavity; this loss rapidly increases with increase in laser output power. Therefore, the output power becomes estimated (see Fig. 4). However, when plan number 2 is applied, $R_1=\infty$, $R_2=10$ meters, $R_3=10$ meters, $\sigma_1\sigma_2=-0.0003$; the cavity is unsteady by itself. When $P=150$ watts, $\sigma_1\sigma_2=0.36<1$; the

with the value of the coefficient α in (1), due to their close proximity to the plane of the resonator mirrors, the cavity is deformed. The beam output power P_{out} and the efficiency η (with respect to the vacuum value) in steady state, $P_{out} = P_{out}(\infty)$, $\eta = \eta(\infty)$, are higher than the rated value of 1.3 mW [1, 2, 3]. This validates the above described calculations.

According to equations (3), (4) and (5), calculate for resonators of the two above-mentioned types the length l_0 of the equivalent chamber and the disorder parameter q_0 , as well as the corresponding dimensions of light spots in the TM_{100} and TM_{110} modes. The values are listed in Table 1.

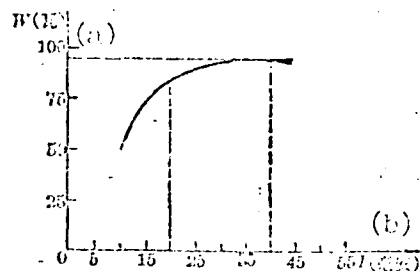


Fig. 4. Output power exhibits saturation during thermal deformation as the steady cavity becomes a wearing cavity (unsteady).
Key: (a) (watts); (b) (milliwatts).

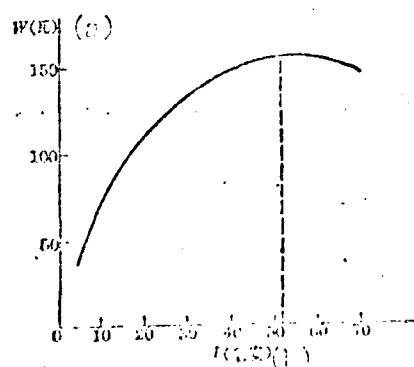


Fig. 5. Output power exhibits an apparent peak when the chamber deforms from an unsteady cavity to a steady cavity. Key: (a) (watts); (b) (milliwatts); (c) (milliwatts).

| $\frac{P_{out}}{P_{in}}$ | 5 | 10 | 15 | 20 | 25 | 30 | 35 | 40 | 45 |
|--------------------------|------|------|------|------|------|------|------|------|------|
| $\frac{P_{out}}{P_{in}}$ | 1.00 | 0.43 | 0.30 | 0.25 | 0.22 | 0.20 | 0.18 | 0.16 | 0.15 |
| $\frac{P_{out}}{P_{in}}$ | 1.00 | 0.43 | 0.30 | 0.25 | 0.22 | 0.20 | 0.18 | 0.16 | 0.15 |
| $\frac{P_{out}}{P_{in}}$ | 1.00 | 0.43 | 0.30 | 0.25 | 0.22 | 0.20 | 0.18 | 0.16 | 0.15 |
| $\frac{P_{out}}{P_{in}}$ | 1.00 | 0.43 | 0.30 | 0.25 | 0.22 | 0.20 | 0.18 | 0.16 | 0.15 |
| $\frac{P_{out}}{P_{in}}$ | 1.00 | 0.43 | 0.30 | 0.25 | 0.22 | 0.20 | 0.18 | 0.16 | 0.15 |
| $\frac{P_{out}}{P_{in}}$ | 1.00 | 0.43 | 0.30 | 0.25 | 0.22 | 0.20 | 0.18 | 0.16 | 0.15 |
| $\frac{P_{out}}{P_{in}}$ | 1.00 | 0.43 | 0.30 | 0.25 | 0.22 | 0.20 | 0.18 | 0.16 | 0.15 |
| $\frac{P_{out}}{P_{in}}$ | 1.00 | 0.43 | 0.30 | 0.25 | 0.22 | 0.20 | 0.18 | 0.16 | 0.15 |
| $\frac{P_{out}}{P_{in}}$ | 1.00 | 0.43 | 0.30 | 0.25 | 0.22 | 0.20 | 0.18 | 0.16 | 0.15 |
| $\frac{P_{out}}{P_{in}}$ | 1.00 | 0.43 | 0.30 | 0.25 | 0.22 | 0.20 | 0.18 | 0.16 | 0.15 |

Key: (a) laser power (watts); (b) output current; (c) (milliwatts).

The above results show the experimental one listed in table 2.

Table 2

| $\frac{P_{out}}{P_{in}}$ | 5 | 10 | 15 | 20 | 25 | 30 | 35 | 40 | 45 | 50 | 55 | 60 |
|--------------------------|------|------|------|------|------|------|------|------|------|------|------|------|
| $\frac{P_{out}}{P_{in}}$ | 20.0 | 22.0 | 24.0 | 26.0 | 28.0 | 30.0 | 32.0 | 34.0 | 36.0 | 38.0 | 40.0 | 42.0 |
| $\frac{P_{out}}{P_{in}}$ | 3.0 | 8.2 | 9.5 | 10.4 | 11.5 | 12.0 | 12.5 | 12.8 | 13.0 | 13.0 | 13.0 | 13.0 |
| $\frac{P_{out}}{P_{in}}$ | 0.0 | 10 | 10 | 10 | 10 | 10 | 10 | 10 | 10 | 10 | 10 | 10 |

Key: (a) laser power (watts); (b) laser power (watts); (c) light-spot diameter (milliwatts); (d) W%.

Plot the above-mentioned experimental results and theoretical calculations onto Figure 6 for comparison. We can see that under low power periods, generally the experimental results and theoretical calculation of mode spot sizes are consistent. When the laser output power is at higher values, the experimental values are greater than the theoretical calculations. The reason for this is that the non-linear effect is gradually increasing with higher values of current. If the laser thermal deformation and non-linear effect are not taken into account, the calculation results are completely different from the experimental results. The calculation results are shown in Figure 6.

By using the relation $\frac{1}{\gamma} = \sqrt{1 - \beta^2}$, $\beta = \frac{v}{c}$, and the above-mentioned approximation, the optical refracting matrix of the above-mentioned system of three lenses can be calculated. It is shown in Fig. 7 that the system of three lenses forms a complete cycle (Fig. 7) of light rays, and the optical refracting matrix [5]:

$$\begin{aligned} \begin{bmatrix} A & B \\ C & D \end{bmatrix} &= \begin{bmatrix} 1 & 0 \\ 0 & 1 \end{bmatrix} \cdot \begin{bmatrix} \cosh \gamma L & \gamma^{-1} \sinh \gamma L \\ \gamma \sinh \gamma L & \cosh \gamma L \end{bmatrix} \\ &\cdot \begin{bmatrix} 1 & 0 \\ -\frac{2}{R_2} & 1 \end{bmatrix} \cdot \begin{bmatrix} \cosh \gamma L & \gamma^{-1} \sinh \gamma L \\ \gamma \sinh \gamma L & \cosh \gamma L \end{bmatrix} \\ &\cdot \begin{bmatrix} 1 & 0 \\ -\frac{2}{R_2} & 1 \end{bmatrix} \cdot \begin{bmatrix} \cosh \gamma L & \gamma^{-1} \sinh \gamma L \\ \gamma \sinh \gamma L & \cosh \gamma L \end{bmatrix} \\ &\cdot \begin{bmatrix} 1 & 0 \\ -\frac{2}{R_3} & 1 \end{bmatrix} \cdot \begin{bmatrix} \cosh \gamma L & \gamma^{-1} \sinh \gamma L \\ \gamma \sinh \gamma L & \cosh \gamma L \end{bmatrix} \\ &\cdot \begin{bmatrix} 1 & 0 \\ -\frac{2}{R_3} & 1 \end{bmatrix} \cdot \begin{bmatrix} \cosh \gamma L & \gamma^{-1} \sinh \gamma L \\ \gamma \sinh \gamma L & \cosh \gamma L \end{bmatrix} \end{aligned}$$

In the equation,

$$R_2' = \frac{R_2 d}{d - R_2 \alpha M_2} = \frac{2LR_2}{2L - 2M\alpha R_2};$$

$$R_3' = \frac{R_3 d}{d - R_3 \alpha M_3} = \frac{2LR_3}{2L - 4M\alpha R_3}$$

Assume $M=150$ volts, $R_2=20.16$ meters, $R_3=10.08$ meters, and the value of γ is approximately estimated as 1.6×10^{-3} per centimeter. Then the above-mentioned matrix value is

$$\begin{bmatrix} -0.0306 & 4.2535 \\ -0.2342 & -0.0285 \end{bmatrix}.$$

Since this optical refracting matrix

$$\begin{bmatrix} A & B \\ C & D \end{bmatrix} = \begin{bmatrix} 2g_1''g_2'' - 1 & 2Lg_1''g_2'' \\ \frac{2}{L}g_1''(g_2'' - 1) & 2g_1''g_2'' - 1 \end{bmatrix}$$

Therefore, $A+(D/2)g_1''g_2''-1$ and $B=2Lg_1''g_2''$. Since this lens series is counted from the center window, $g_1''=0$ and, by analogy, the above condition, we derive $g_2''=0.455$ and $L=4.13$ meters; L_0 is the distance of the center of the lens cluster. By using similar relations (2), we derive the radius (or the light spot in the L_0 plane) of 2.4×10^{-3} meters or about 2.4×10^{-3} mm. Then,

For the 100 W power, the calculated maximum temperature of the film is 120°C , which is very close to the experimental value of 110°C .

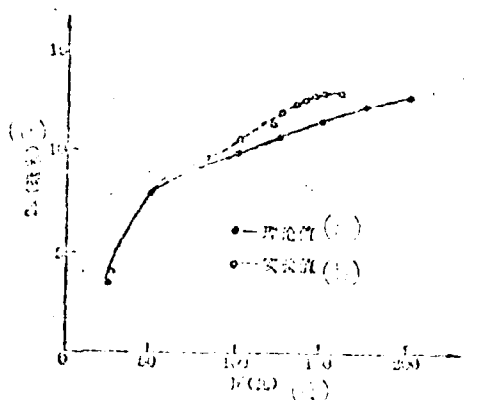


Fig. 6. Comparison between theoretical calculation and experimental results of the laser output light intensity.
Key: (a) theoretical value; (b) experimental results; (c) (11th section); (d) (watts).

$$R_1 = \infty \quad f_1 = \frac{R_1}{2} \quad f_2 = \frac{R_2}{2} \quad f_3 = \frac{R_3}{2} \quad R_4 = \infty$$

$$\left[\begin{array}{c} \text{---} L_1 \text{---} \text{---} L_2 \text{---} \text{---} L_3 \text{---} \end{array} \right]$$

$$R_1 = \infty \quad \left[\text{---} L_1 \text{---} \right] R_2$$

Fig. 7. One period of lens series and its equivalent two-lens chamber as the space is filled with lens-like medium.

V. Discussion

If the value of a lens is relatively high and the coefficient of thermal expansion and conductivity are relatively large, we cannot neglect the effect of mirror thermal deformation on laser resonator parameters. In particular, for a folded CO_2 laser with output power greater than 100 watts, in order to commercialize the laser and to obtain the longest of plane discharge tube and mirror length, the thermal deformation of the effect of mirror thermal deformation must be taken into account. The following is a brief discussion.

FOLED RESONATOR FOR HIGH-POWER LASERS

Lei Shizhan, and Zhou Shuangji

Shanghai Institute of Cyber and Fine Mechanics, Chinese Academy of Sciences

Submitted 7 April 1986

Using ray transfer matrix, we have computed beam radii and mode volumes in the folded resonator and the dependence on mirror curvature of resonator and the parameter a of the gas plasma negative lens. Results indicate that folded resonator configuration used in a laser with longer plasma length, not only reduces space length of the device, but also possesses significance for obtaining stable high-power output taking into account of the effect of negative plasma lens.

The folded resonator configuration is often used in some high-power lasers, such as gas dynamic laser, chemical laser, high-speed flow gas laser, dye laser, and sealed-carbonized high power CO_2 molecule laser. Especially for CO_2 molecule laser, adoption of the folded chamber not only reduces the spatial length of apparatus, but the output power of the apparatus can also be higher than that of the unfolded configuration. In paper [1], there is a discussion on a volume calculation of a resonator composed of three mirrors. However, there is no consideration given to the lens effect of the negative plasma; this is a very important question. The high-power lasers, during laser oscillation, the electron and ionization is always considered to thermal energy to increase the temperature of the gas. This is an inevitable fact. In the cavity of the laser,

10

$$\begin{aligned}
T_{12} &= \begin{pmatrix} \cosh(al), & a^{-1} \sinh(al) \\ a \sinh(al), & \cosh(al) \end{pmatrix} \\
T_{13} &= \begin{pmatrix} 1, & 0 \\ -2/R_1, & 1 \end{pmatrix}; \\
T_{17} &= \begin{pmatrix} \cosh(al), & a^{-1} \sinh(al) \\ a \sinh(al), & \cosh(al) \end{pmatrix}; \\
T_{18} &= \begin{pmatrix} 1, & 0 \\ -2/R_1, & 1 \end{pmatrix}; \\
T_{19} &= \begin{pmatrix} \cosh(al), & a^{-1} \sinh(al) \\ a \sinh(al), & \cosh(al) \end{pmatrix}.
\end{aligned}$$

The radius ω of the light spot of the beam in the cavity is

$$\omega^2 = \frac{2\lambda R}{\pi} \sqrt{1 - (1/D)^2}.$$

The volume of the laser mode is

$$V = \pi \int_0^l \omega^2(z) dz$$

In the equation, λ is wavelength; a is the diametrically distributed parameter of refractivity ($a = \sqrt{\epsilon_0/\epsilon_0}$); the diametrical distribution of refractivity n takes the form of $n = n_0 + (1/4)n_2 r^2$. A TI-16 electronic computer was used for the numerical computation.

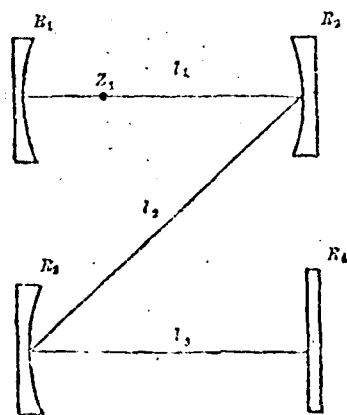


Fig. 1. Folded optical resonator.

Figures 3 through 5 show the relationship between the radius of curvature of the filament, r , and the radius of the fiber on the fiber bed, V , of the filament for different a . Figures 3 and 4 show the variations in the radius of curvature of r with the filament radius a and mole volume V for fixed values of $b = 10^{-4}$ and 10^{-5} centimeters, $l = 240$ centimeters, and $l_0 = 20$ centimeters.

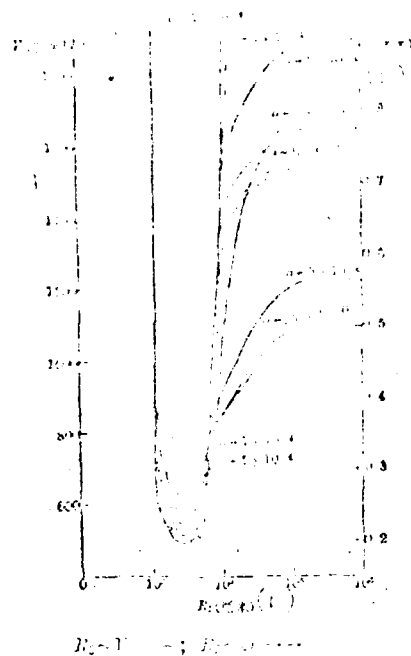


Fig. 3. Relationship between R_3 on one hand, and R_2 (resonator radius and mode volume) on the other.
Key: (1) ($\alpha=0.2$); (2) ($\alpha=0.3$); (3) ($\alpha=0.4$); (4) ($\alpha=0.5$); (5) ($\alpha=0.7$); (6) ($\alpha=1.0$).

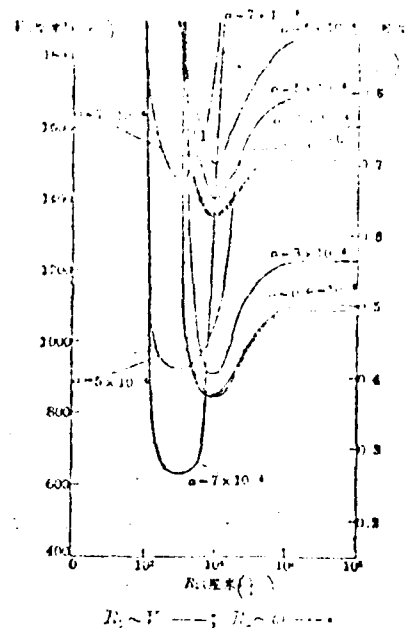


Fig. 4. Relationship between R_3 on one hand, and R_2 (resonator radius and mode volume) on the other ($R_3=10^6$ centimeters).
Key: (1) ($\alpha=0.2$); (2) ($\alpha=0.3$); (3) ($\alpha=0.4$); (4) ($\alpha=0.5$); (5) ($\alpha=0.7$); (6) ($\alpha=1.0$).

Apparently, these changes are the same; the mode volume is very small at $R_3=10^2$. As the value of the condition of the rate R_3 value, the mode volume at $R_2=10^6$ cm is greater than 10^4 cm. However, when the value of α is relatively large ($\alpha=1.0$), it is easier to let the mode volume of resonator approach infinity; i.e., the mode volume tends to enter the high-loss zone of light output power. According to the results from Figures 3 and 4, when $R_2=10^6$ and $\alpha=1.0$, even R_3 is as great as 10^6 cm; the resonator is still in the low-loss region. However, when $R_2=10^6$ cm, R_3 is only limited to a value in the vicinity of 10^4 cm and the conversion of light power in the resonator is then relatively low. In addition, we can see from Fig. 5 that R_3 changes from 10^2 to 10^6 cm and the change of mode volume is small when R_2 is taken as 10^6 cm. However, the stability requirement of the resonator (the radius of curvature) is higher since misalignment can be caused with slight vibration of the resonator. From the above analysis, we can see that the value of R_3 and the frequency can be well chosen for R_2 .

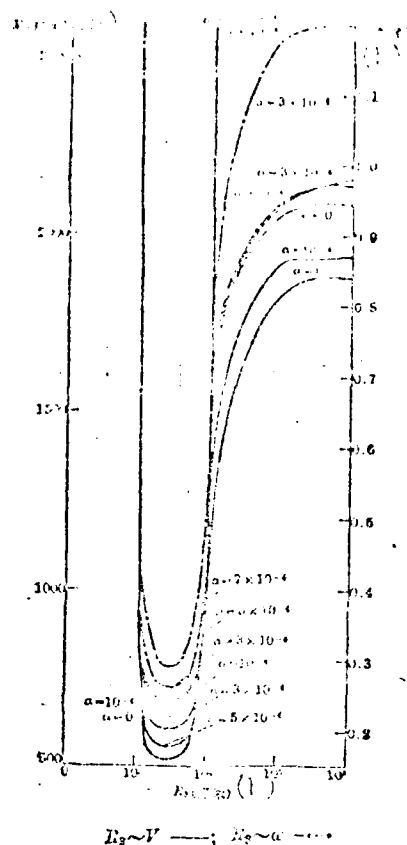


Fig. 4. Relationship between R_2 on one hand, and light-ray radius of curvature volume on the other (in cm^2 and meters). Key: (a) (cubic centimeters); (b) (centimeters).

We can see from the results in Figures 2 to 5 that assuming the condition of the same radius of curvature of the mirrors at both resonator ends, the mode volume of the folded chamber is smaller than that for the non-folded chamber. From this point, adoption of the folded resonator configuration does not tend to increase laser efficiency. However, as there is a negative lens effect in the laser working medium, if the folded resonator configuration is not adopted, the loss of light power in the laser is increased by 10% (due to an overlarge curvature of light-ray axis); the resonator pump is still related to a lower level in order to obtain the necessary gain effect (reduction of the a value). We can see from the results in Fig. 4 that by adopting the folded resonator for

...the first set of data is adopted in a resonator, the mode volume is greater than for the third-set of data. However, the power obtained by using the third-set data is much greater than for the first set. From the calculated results listed in Fig. 5, for the resonator of the first-set data, the mode volume is too large; i.e., the loss is too high. For the resonator of the second-set data, the corresponding mode volume is too small, so this is also not suitable. Hence, the laser output power is also the lowest.

This point is also proved experimentally. The following table shows the output power for different radii of curvature in a three-turn resonator.

| $R_1(\text{cm})$ | 1.8×10^4 | 1.8×10^4 | 1.25×10^4 |
|------------------|-------------------|-------------------|--------------------|
| $R_2(\text{cm})$ | ∞ | 10^4 | ∞ |
| $R_3(\text{cm})$ | ∞ | 10^4 | 10^4 |
| $R_4(\text{cm})$ | ∞ | ∞ | ∞ |
| Output (a) | 20 | 50 | 250~300 |

Key: (a) Centimeters; (b)
Output power (watts).

When the first set of data is adopted in a resonator, the mode volume is greater than for the third-set of data. However, the power obtained by using the third-set data is much greater than for the first set. From the calculated results listed in Fig. 5, for the resonator of the first-set data, the mode volume is too large; i.e., the loss is too high. For the resonator of the second-set data, the corresponding mode volume is too small, so this is also not suitable. Hence, the laser output power is also the lowest.

Figure 6 shows the relationship among the beam light spot radius, mode volume, and a value of the laser working medium. We can see from the figure that the larger the radius of curvature of the turning mirror, the smaller the allowable range of a values. However, the a value is determined by the laser working medium; the larger

Fig. 6(a). Relationship between light-spot radius and a : (in the figure, curves for $l=0$ and $l=711$, 235 represent, respectively, light-spot radius of mirror R_1 , and the values of light spots at distances of 711 and 235 cm from mirror R_1)

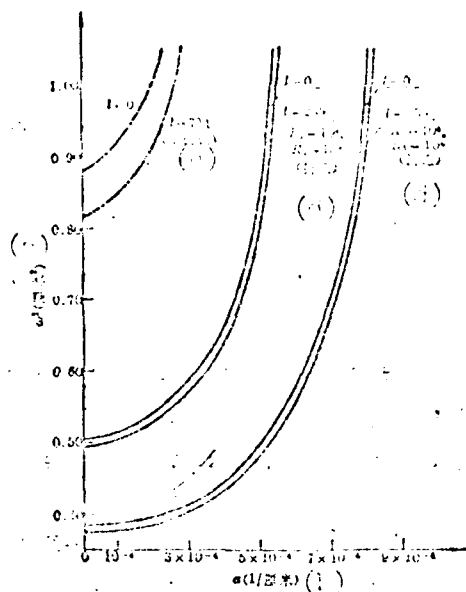


Fig. 6(a). Relationship between light-spot radius and a : (in the figure, curves for $l=0$ and $l=711$, 235 represent, respectively, light-spot radius of mirror R_1 , and the values of light spots at distances of 711 and 235 cm from mirror R_1)

Key: (a) (square centimeter); (b) (1/centimeter); (c) (not folded); (d) (folded).

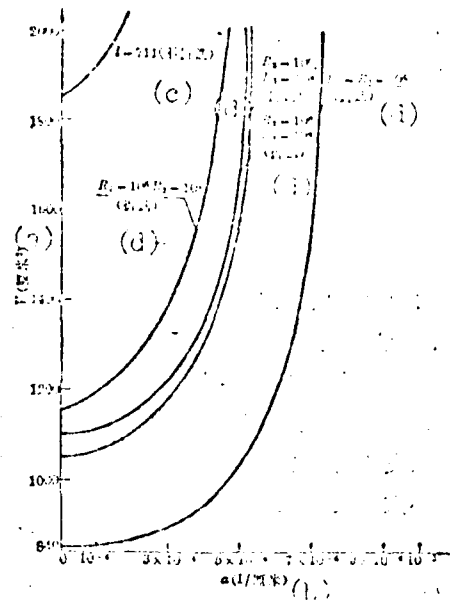


Fig. 6(b). Relationship between mode volume and a .

Key: (a) (cubic centimeter); (b) (1/centimeter); (c) (not folded); (d) (folded).

Therefore, when designing a resonator, it is appropriate to choose spherical mirrors as light-turning mirrors; as for the R_2 and R_3 values, they are related to the length of each folded element. By using the light transmission matrix and its standard calculation procedure, a comparison calculation can be made to the mode volume and in-diameter term; thus, suitable values can be chosen.

111-112

1. Yul't, G. I., and others: *Usp. fiz. nauk*, 1971, 14, 125.
2. Galich, P. K. V., et al: *Usp. fiz. nauk*, 1970, 9, 1755.
3. Zhurav, M. I.: *Usp. fiz. nauk* (JOURNAL OF PHYSICS), 1974, 23, 437.

A COPPER VAPOR LASER

Liang Paogen, Jing Chunyang, Zhang Guiyan,
Yin Xianhua, Cong Yunching, and Han Sanyichen

Shanghai Institute of Optics and Fine Mechanics, Chinese Academy of
Sciences

Submitted 30 November 1979

With copper vapor or copper halide vapor as laser medium, excited by high repetition frequency resonance Blumlein discharge circuit, laser output are obtained at 5136 Å and 5782 Å. For charge capacitance of 1.5 nF, charge voltage of 6000 V and a repetition rate of 16 kHz, the average output laser power is 1.2 W.

1. Introduction

Among pulsed metal vapor lasers, the atomic copper vapor laser is a typical type. The copper vapor laser requires relatively high working temperatures and excitation with short pulses; there are a series of technical difficulties. In the past, people were not interested in the development of copper vapor lasers. Until 1972 after Soviet researchers successfully manufactured implements with an average power of 25 watts [1], the general attitude was changed in a wave of improving and developing copper and other metal vapor lasers. In 1973, an American used copper halide to replace copper as the working medium in considerably reducing the required working

[illegible](17) *Experiments in the Extended Translation*

Copper halides provide vapor is selected as the larer working medium. We know generally that metal vapor has very low vapor pressure at room temperature and copper is one such metal. However, for resonant self-excited capture, the minimum vapor density of 10^{13} cm⁻³ is required for a 1-cm diameter tube. This vapor density can only be attained at high temperatures. For copper halides, the temperature required to attain this vapor density is 300-600°C as we applied discharge self-heating method to carry it out. For pure copper, it is required to heat to above 1500°C. We used an electric furnace outside a discharge tube to first heat the copper to 1000 °g. Then after discharge, the pure copper heated spontaneously to a high temperature above 1500°C.

An quartz tube of $\phi 8 \times 12$ and a ceramic aluminate tube were used to construct the discharge tube; the distance between electrodes is 250,300 mm; connections between ceramic tungsten electrode and quartz tube employed molybdenum seals. Two terminals of discharge tube were ground into a quartz bragg angle. In a copper halide vapor laser, copper halide was placed in a side tube at a middle of discharge tube. For a pure copper vapor laser, the copper powder is uniformly placed axially along the ceramic aluminate tube; in the tube 20 Torr of neon is filled as a buffer gas. The discharge zone uses a vacuum jacket sleeve or asbestos cloth as insulation.

The resonator is composed of a mirror of multilayer medium. The (100) surface of crystal is with total reflection to 5106\AA and a (100) surface of copper is (or a thin multilayer medium)

The circuit diagram of the proposed very pulse generator 100, shown in Fig. 1, consists of two main sections: a charging section and a discharge section. The charging section includes a transformer 110, a capacitor 120, and a thyristor 130. The discharge section includes a capacitor 140, an inductor 150, and a thyristor 160. The circuit is controlled by a control pulse thyristron 170. The frequency of the control pulse thyristron was used to charge and discharge at the multiple repetition frequency. A $20X_1-8U/16$ pulse thyristron was picked as the switching element with grid trigger pulse supplied by the pulse transformer output level which connected to a $20X_1-3.5/3$ thyristron. The pulse transformer was controlled by an adjustable frequency pulse signal generator. After capacitance C resonantly charged to voltage U_0 through inductance L, discharge began from the capacitor through the control pulse thyristron and its characteristic frequency for oscillation. The voltage at capacitor C was lowered from the full value U_0 to negative $-U_0$ through zero. If at this time, no circuit is connected to the laser tube, the potential difference of two electrodes can attain a value twice as large as U_0 . After cooperation with the laser tube, capacitor C discharged with current I through the (laser's) inductance, capacitance, pure resistance, and circuit stray inductance. Since at this time thyristron was open, the thyristron open and closing time had no effect on the laser tube discharge circuit. A higher efficiency can be attained with proper matching of circuit and laser tube.

Figure 2 shows the voltage waveform of charges and electrons. We can see from the figure that the charge voltage rises approximately 1.1-1.14 eV; this is because an electron incident from above is reflected back and the electric potential barrier from a p-n junction is not strong and the electron voltage is less than the contact voltage.

light source. The discharge current was measured by means of a Rogowski coil connected to a current transformer. A resistive load was connected with the coil in the circuit to measure the discharge current waveform (Fig. 3). The discharge current was 100 amperes. The measurement of voltage and current waveform was performed when the discharge capacitance was 0.3 microfarads, charge voltage at 3500 volts, pulse repetition frequency at 10 kilohertz, and an 4.8x250 laser tube was used.

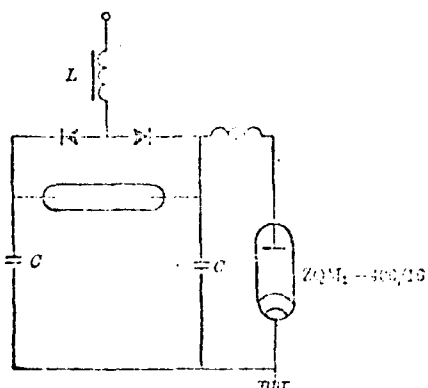


Fig. 1. Schematic diagram of charge and discharge circuit.

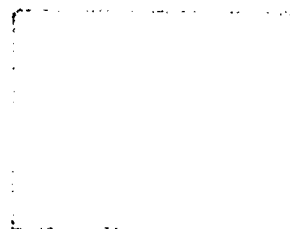


Fig. 2. Voltage waveform at charge and discharge: time scale at 0.1 millisecond per centimeter.



Fig. 3. Charge current waveform: amplitude at 10 volts per centimeter and time scale at 50 nanoseconds per centimeter.

For copper hollow-cathode laser, the average laser output power is 2.2 watts for an internal laser tube diameter of 32 pole-to-pole distance of 361 millimeters, charge capacitance at 1.5 nano-seconds, charge voltage of 6000 volts, and pulse repetition frequency at 10 kilohertz.

For a pure copper vapor laser (48x250), the average laser output power is 150 milliwatts with charge capacitance at 2 nanofarads, charge voltage at 6000 volts, and pulse repetition frequency at 10 kilohertz.

A circular-disk monochromator (with removal of a narrow exit slit) was used for photographing 5106 \AA and 5782 \AA spectral lines (Fig. 4). In the figure, the mercury spectral line is used as a comparison line.

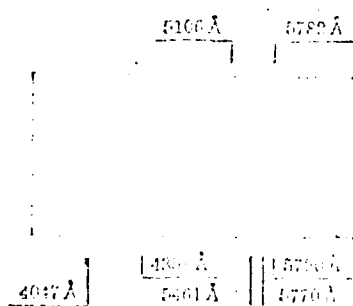


Fig. 4. Light spectra: 1) line for 5100 Å; 2) and 3) 5120 Å mercury line in the absence (upper line).

a) $\frac{1}{2} \cdot 100 = 50$

b) $1.1 \cdot 10^{-1}$ g/L, 30

During the experiment it was found that the incessant wearing of copper hollow during the working process is an important factor why this type of laser apparatus has a short life-span. Under the precondition of correctly controlling temperatures, an increase of the filling medium is the most direct method of extending the laser emission service life. The filling medium of our laser ($\Phi 8 \times 250$) amounted to about 2 grams and the stabilized light-emitting duration was more than 15 hours. During the later period of the service life of this type of laser, often the (relatively intensive) discharge channel is quivering, bending, and narrowing; this is relatively closely related to the electrophoresis effect during the discharge process. The electrophoresis effect causes the density of copper particles to gradually decrease in the discharge channel. In a situation where there is no timely supply of the filling medium, E/N gradually increases, causing an unstable discharge electrode, or even suddenly extinguishing it.

D. TROTSKY, *S. A., I PR.*; *PISTUN V ZHITIE*, 1970, 16, No. 1, 40.

1. The first part of the report is a general introduction to the subject of the study. It discusses the importance of the study and the objectives of the research.

SCIENCE NOTES: ULTRAVIOLET PRE-IONIZATION DISCHARGE PUMP APT LASER

Fu Shufen, Chen Jianwen, and Liu Minzhong

Shanghai Institute of Optics and Fine Mechanics, Chinese Academy of Sciences

On an ultraviolet pre-ionization high-gas-pressure laser, we successfully achieved APT laser oscillation. The experimental installation is shown in Fig. 1. The discharge chamber is a nylon circular cylinder one meter long, with an internal diameter of 76 millimeters. A thin-shell aluminum flange was used to directly connect an optical resonator sheet onto two cylinder terminals. By use of an elastic (deformation adjustment) cavity sheet of the flange, it is conveniently adjusted with stable characteristics. In addition, the effect of absorption by the atmosphere layer (in the external cavity type apparatus) on laser wavelength can be avoided.

The main discharge electrode is brass; its surface is cylindrical with 4.1 millimeter. This round, smooth electrode with small radius can lead to uniform discharges and to strengthen the density of the excitation power. The parallel-plate capacitor consists of two 0.5-mm-thick electrolyte copper film with a dielectric of 0.5-mm polyethylene film. The adjustable distance between the electrodes

the laser is a cylindrical resonator 1.5 m long, filled with a gas mixture of 0.2% NF_3 , 12% Ar, and 87.8% He. The laser is pre-ionized by a 10 kV discharge. The main discharge is initiated by a 10 kV spark. The laser output is 1.5 m long. The equivalent circuit of the system is shown in Fig. 2.

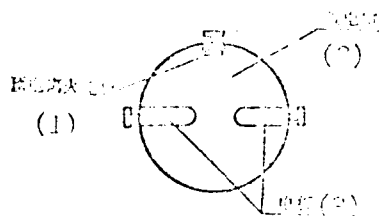


Fig. 1. Cross-sectional diagram of ultraviolet pre-ionized ArF laser.
Key: (1) Pre-ionization spark plate; (2) Discharge chimney; (3) Electrode plate.

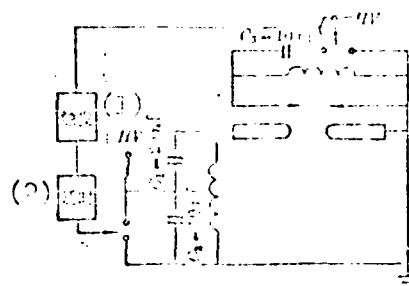


Fig. 2. Equivalent circuit of laser system.
Key: (1) Triggering; (2) Delayed.

When the main discharge and charge are 20 kilovolts, the total input energy is 6 joules. The delay time between main discharge and pre-ionization is a very important parameter; the selection of the best delay time relies on the pre-ionization capacitance, charge voltage, constituents of gas filled, and gas pressure.

The gas mixture is NF_3 :Ar:He=0.2%:12%:87.8%; laser outputs were obtained at a total gas pressure of 1.5-2.5 atmospheric pressures. Figure 3 shows a blackness curve of the ArF laser spectrum, photographed with a 2-meter grating spectrophotograph; the total width at half intensity is 3A.

Compared with XeF and XeCl, the service life of the ArF laser is considerably shorter; this is mainly because of light-absorbed impurities in the discharge. In order to obtain long service life and

It is not clear why the 1940-41 season is so short. It may be that the 1940-41 season is the first with a short low season, the summer months, and the 1941-42 (which is going) has a long low season. For various collections of short- and long-term interest the American is going to be a good, low in price and probably a high-value-for-money item.

Fig. 3. Blackness curve of ArF laser spectrum

LITERATURE

EXPERIMENTAL AND RESEARCH OF ELECTRON BEAM CONTROL XeCl QUASI-MOLECULE LASER

Hong Pu

Institute of Electronics, Chinese Academy of Sciences

We built a large volume (10 liters) electron beam lateral pump and electron beam-controlled discharge laser; Fig. 1 shows the schematic diagram of the laser structure.

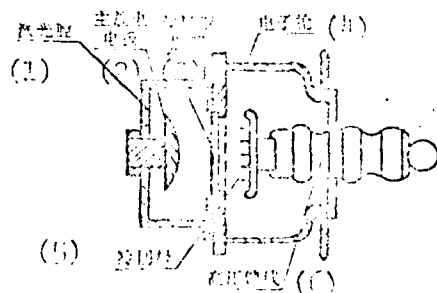


Fig. 1. Schematic diagram of structure.

Key: (1) Lower chamber; (2) Main discharge electrode; (3) Pre-discharge electrode; (4) Electron gun; (5) Cold cathode; (6) High voltage ion pump feed line.

The laser resonator is a cylindrical discharge chamber with a diameter of 10 centimeters and a length of 1.5 meters. The electrodes are located at the ends of the chamber. The discharge is initiated by a high-voltage pulse generator.

The laser resonator is a cylindrical discharge chamber, whose diameter is 10 centimeters and whose length is 1.5 meters. The electrodes are located at the ends of the chamber. The discharge is initiated by a high-voltage pulse generator. The distance between the electrodes is 1.5 meters. The chamber has two plane mirrors with a diameter of 9 centimeters. The mirrors have two standard diameters which are 5.7 centimeters and 12 centimeters respectively. The mirrors are coated with a multi-layer-medium film, mirror spacing is 1.5 meters. One mirror has a total reflection of 3080\AA (reflectivity over 99 percent) and the other mirror has a reflectivity of 82 percent, constituting an optical resonator.

The anode of the laser resonator is a solid aluminum ring electrode. There are two values for the distance between the electrodes. When $d=5.7$ centimeters, the discharge volume of the laser resonator is 5.7 liters; when $d=9$ centimeters, the discharge volume of the laser resonator is 9 liters. The power source for the main discharge is composed of four parallel capacitors of 0.5 microfarad and 50 kilovolts.

In the experiment, HCl was used as the chlorine source. Ar was used as a diluting agent; the mixing ratio is $\text{Ar/Xe/HCl}=95.8/3.8/0.4$. The total pressure was one atmospheric pressure. At the side of the total reflection mirror (rate of transparency 0.2 percent) of the laser resonator; the laser spectrum was obtained by photography. When a low-pressure mercury lamp is used as standard spectrum, Fig. 2 shows the photographed spectral lines and Fig. 3 shows the spectral density curve after measurement. From Fig. 3, the laser spectra are clearly seen with wavelengths at 3080\AA and 3082\AA .

FILMED
4-8